VIETNAM NATIONAL UNIVERSITY, HANOI

UNIVERSITY OF ENGINEERING AND TECHNOLOGY

MAN DUC CHUC

RESEARCH ON LAND-COVER CLASSIFICATION METHODOLOGIES FOR OPTICAL SATELLITE IMAGES

MASTER THESIS IN COMPUTER SCIENCE

Hanoi – 2017

VIETNAM NATIONAL UNIVERSITY, HANOI
UNIVERSITY OF ENGINEERING AND TECHNOLOGY

MAN DUC CHUC

RESEARCH ON LAND-COVER CLASSIFICATION METHODOLOGIES FOR OPTICAL SATELLITE IMAGES

DEPARTMENT: COMPUTER SCIENCE
MAJOR: COMPUTER SCIENCE
CODE: 60480101

MASTER THESIS IN COMPUTER SCIENCE
SUPERVISOR: Dr. NGUYEN THI NHAT THANH

Hanoi – 2017

PLEDGE

I hereby undertake that the content of the thesis: “Research on Land-Cover classification methodologies for optical satellite images” is the research I have conducted under the supervision of Dr. Nguyen Thi Nhat Thanh. In the whole content of the dissertation, what is presented is what I learned and developed from the previous studies. All of the references are legible and legally quoted.

I am responsible for my assurance.

Hanoi, day month year 2017

Thesis’s author

Man Duc Chuc

ACKNOWLEDGEMENTS

I would like to express my deep gratitude to my supervisor, Dr. Nguyen Thi Nhat Thanh. She has given me the opportunity to pursue research in my favorite field. During the dissertation, she has given me valuable suggestions on the subject, and useful advices so that I could finish my dissertation.

I sincerely thank the lecturers in the Faculty of Information Technology, University of Engineering and Technology - Vietnam National University Hanoi, and FIMO Center for teaching me valuable knowledge and experience during my research.

Finally, I would like to thank my family, my friends, and those who have supported and encouraged me.

This work was supported by the Space Technology Program of Vietnam under Grant VT-UD/06/16-20.

Hanoi, day month year 2017

Man Duc Chuc

Content

CHAPTER 1. INTRODUCTION

1.1. Motivation

Remotely-sensed images have been used for a long time in both military and civilization applications. The images could be collected from satellites, airborne platforms or Unmanned Aerial Vehicles (UAVs). Among the three, satellite images have gained popularity due to large coverage, available data and so on. In general, remotely-sensed images store information about Earth object's reflectance of lights, i.e. Sun's light in passive remote sensing [1]. Therefore, the images contain itself lots of valuable information of the Earth's surface or even under the surface.

Applications of remotely-sensed images are diverse. For example, satellite images could be used in agriculture, forestry, geology, hydrology, sea ice, land cover mapping, ocean and coastal [1]. In agriculture, two important tasks are crop type mapping and crop monitoring. Crop type mapping is the process of identification crops and its distribution over an area. This is the first step to crop monitoring which includes crop yield estimation, crop condition assessment, and so on. To these aims, satellite images are efficient and reliable means to derive the required information [1]. In forestry, potential applications could be deforestation mapping, species identification and forest fire mapping. In the forest where human access is restricted, satellite imagery is an unique source of

information for management and monitoring purposes. In geology, satellite images could be used for structural mapping and terrain analysis. In hydrology, some possible applications cloud be flood delineation and mapping, river change detection, irrigation canal leakage detection, wetlands mapping and monitoring, soil moisture monitoring, and a lot of other researches. Iceberg detection and tracking is also done via satellite data. Furthermore, air pollution and meteorological monitoring could be possible from satellite perspective. In general, many of the applications more or less relate to land cover mapping, i.e. agriculture, flood mapping, forest mapping, sea ice mapping, and so on.

Land cover (LC) is a term that refers to the material that lies above the surface of the Earth. Some examples of land covers are: plants, buildings, water and clouds. Land cover is the thing that reflects or radiates the Sun's lights which then be captured by the satellite's sensors. Land use and land cover classification (LULCC) has been considering as one of the most traditional and important applications in remote sensing since LULCC products are essential for a variety of environmental applications [2].

Regarding land cover classification (LCC), there are currently many researches around the world. These researches could be categorized by several criteria such as geographical scale of classification, multiple land covers classification or single land cover classification. For the former, LCC can be classified into regional or global studies. Regional studies focus on investigating LCC methods

for one or more specific regions. Global studies concern classification at global scale.

Although there are many efforts to map land covers globally, the LC accuracies are still much lower than regional LC maps. This is understandable as there are many challenges in LCC at global scale including diversity of land-cover types, lack of ground-truth data, and so on [3]. In regional studies, the difficulties are more or less reduced, thus resulting in more accurate LC maps. Some typical regional LC studies could be mentioned, i.e. Hannes et al. investigated Landsat time series (2009 - 2012) for separating cropland and pasture in a heterogeneous Brazilian savannah landscape using random forest classifier and achieved and overall accuracy of 93% [4]. Xiaoping Zhang et al. used Landsat data to monitor impervious surface dynamics at Zhoushan islands from 2006 to 2011 and achieved overall accuracies of 86-88% [5]. Arvor et al. classified five crops in the state of Mato Grosso, Brazil using MODIS EVI time series and their OAs ranged from 74 – 85.5% [6].

Although land-cover classification (LCC) mapping at medium to high spatial resolution is now easier due to availability of medium/high spatial resolution imagery such as Landsat 5/7/8 [7], in cloud-prone areas, deriving high resolution LCC maps from optical imagery is challenging because of infrequent satellite revisits and lack of cloud-free data. This is even more pronounced in land cover with high temporal dynamics, i.e. paddy rice or seasonal crops, which require observation of key growing stages to correctly identify [8], [9].

Vietnam is located in a tropical monsoon climate frequently covered by cloud [10], [11]. Some studies used high temporal resolution but low spatial resolution images (MODIS) [12]. Some studies employed single-image classifications [13]. However, common challenges of mono-temporal approaches include misclassification between bare land or impervious surface and vegetation cover type [14]. Whereas land cover classification using cloud-free Landsat scenes may lack enough observations to capture temporal dynamics of land-cover types.

1.2. Objectives, contributions and thesis structure

To date, land cover classification in cloud-prone areas is challenging. Furthermore, efficient LC methods for the regions, especially for areas with high temporal dynamics of land covers, are still limited. In this thesis, the aim is to propose a classification method for cloud-prone areas with high temporal dynamics of land-cover types. It is also the main contribution of the research to current development of land cover classification. To assess its classification performance, the proposed method is first tested in Hanoi, the capital city of Vietnam. Hanoi is one of the cloudiest areas on Earth and has diverse land covers. In particular, the results of this thesis could be applicable to other cloudy regions worldwide and to clearer ones also.

This thesis is organized into five chapters. In chapter 1, I give an introduction to remotely-sensed data and its application in various domains. A problem statement is also presented. Theoretical backgrounds in remote sensing, compositing methods and land cover

classification methods are introduced in Chapter 2. Proposed method is presented in Chapter 3. Chapter 4 details experiments and results. Finally, some conclusions of my thesis are drawn in Chapter 5.

CHAPTER 2. THEORETICAL BACKGROUND

2.1. Remote sensing concepts

Remote sensing is a science and art that acquires information about an object, an area or a phenomenon through the analysis of material obtained by specialized devices. These devices do not have a direct contact with the subject, area, or studied phenomena.

Electromagnetic waves that are reflected or radiated from an object are the main source of information in remote sensing. A remote sensing image provides information about the objects in form of radiated energy in recorded wavelengths. Measurements and analyses of the spectral reflectance allow extraction of useful information of the ground. Equipments used to sense the electromagnetic waves are called sensor. Sensors are cameras or scanners mounted on carrying platforms. Platforms carrying sensors are called carrier, which can be airplanes, balloons, shuttles, or satellites. Figure 1 shows a typical scheme for remote sensing image acquisition. The main source of energy used in remote sensing is solar radiation. The electromagnetic waves are sensed by the sensor on the receiving carrier. Information

about the reflected energy could be processed and applied in many fields such as agriculture, forestry, geology, meteorology, environments and so on.

A remote sensing system works in the following model: a beam of light, emitted by the sun/the satellite itself, firstly reaches the Earth surface. It is then partially absorbed, reflected and radiated back to the atmosphere. In the atmosphere, the beam may also be absorbed, reflected or radiated for another time. On the sky, the satellite's sensor will pick up the beam that is reflected back to it. After that it is the process of transmitting, receiving, processing and converting the radiated energy into image data. Finally, interpretation and analysis of the image is done to apply in real-life applications

2.2. Satellite images

Satellite images are images of Earth or other planets collected by observation satellites. The satellites are often operated by governmental agencies or businesses around the world. There are currently many Earth observation satellites and they have common characteristics including spatial resolution, spectral resolution, radiometric resolution and temporal resolution.

2.3. Compositing methods

Optical satellite images have a big drawback. In particular, they are heavily impacted by clouds. If a region is covered by clouds during its satellite passing time, the recorded data is considered lost. Therefore, methods for tackling clouds in optical satellite images have

been studied by many researchers. Pixel-based image compositing is a paradigm in remote sensing science that focuses on creating cloud-free, radiometrically and phenologically consistent image composites. The image composites are spatially contiguous over large areas [15]. In the past, some compositing methods for low spatial resolution images (i.e. 500x500m or greater) were developed [16], [17]. Those methods were used primarily to reduce the impacts of clouds, aerosol contamination, data volume and view angle effects which are inherent in the images. Due to high temporal resolution of the satellites, the compositing methods were relatively simple, i.e. use maximum Normalized Difference Vegetation Index (NDVI) or minimum view angle to pick an appropriate observation for a target pixel. Since the opening of the Landsat archive, compositing methods for Landsat images have been developed and benefitted by pre-existing approaches for MODIS and AVHRR data.

Recently, a number of best-available-pixel compositing (BAP) methods have been proposed for medium/high satellite images. Generally, BAP methods replace cloudy pixels with best-quality pixels from a set of candidates through rule-based procedures. Selection rules are based on spectral-related information, that is, maximum normalized difference vegetation index (NDVI) [18] and median near-infrared (NIR) [19]. On another approach, Griffiths et al. proposed a BAP method ranking candidate pixels by score set such as distance to cloud/cloud shadow, year, and day-of-year (DOY) [20]. This method was improved by incorporating new scores for atmospheric opacity and sensor types [15]. Gómez et al. recently offered a review

emphasizing BAP potential for monitoring in cloud-persistent areas [21], which includes applications in forest biomass, recovery and species mapping [22]–[24], change detection applications [25], and general land-cover applications [26].

2.4. Machine learning methods in land cover study

Basically, LC classification is a type of classification on image data. Therefore, machine learning classifiers are also applicable to LC classification. In fact, there existed a huge amount of researches on machine learning classifiers in LCC. These methods range from simple thresholding to more advanced approaches such as maximum likelihood, logistic regression, decision tree (ID3, C4.5, C5), random forest, support vector machine (SVM), artificial neuron network (ANN) and so on [27]–[31], ensemble methods and deep learning.

CHAPTER 3. PROPOSE LAND-COVER STUDY METHODOLOGY

3.1. Study area

Hanoi is the capital of Vietnam, the country's second largest city covering approximately 3,300 km2, located in the centre of Red River Delta (RRD). Hanoi has three basic kinds of terrain including a fertile delta, midland region and mountainous zone. Hanoi is mainly divided into agricultural area (56.6%) and non-agricultural area (40.6%) in 2010 [32]. In agricultural areas, paddy rice is dominant (60.9%) followed by other crops such as maize as well as various vegetable crops. Paddy rice is planted two times per year, while crops are grown in other dedicated areas. Occasionally, short-season vegetable crops or aquaculture are grown before the start of the first rice season. Non-agricultural areas are mostly covered by impervious surfaces and mosaicked natural landscape. Accordingly, I investigate seven LC classes for Hanoi including paddy rice, cropland, grass/shrub, trees, bare land, impervious area and water body.

3.2. Data collection

3.2.1. Reference data

Official land-use data from Hanoi Environment and Natural Resources Department is used for training and testing data selection

[33]. The selection procedure is based on stratified random sampling method. This is done separately for training and testing data. And these datasets are guaranteed to share no same point on the ground. Since different land uses may contain the same land-cover types, I therefore generated 11 strata labelled as bare area, long-term crops, short-term crops, forest, grass, impervious area, mudflats, rice, water, others and overlap areas of the land use strata. Training and testing data are randomly sampled from the strata and then labelled into 7 classes using high resolution images of Google Earth and field data (Figure 12). Total numbers of training and testing data are 5079 and 2748 points

3.2.2. *Landsat 8 SR data*

To prepare imagery for the 2016 Hanoi land cover map, all Landsat 8 Surface Reflectance (L8SR) images from 2013 to 2016 are collected from USGS Earth Explorer (https://earthexplorer.usgs.gov/). There are 54 available L8SR scenes which are not 100% cloud-contaminated. As Hanoi is covered by two consecutive L8SR scenes per revisit, the resulting 27 images are mosaicked.

3.2.3. Ancillary data

Another ancillary data in this study is rice area statistics in 2016 produced by Hanoi Statistics Office (http://thongkehanoi.gov.vn/). This statistics include rice planting area at provincial level. The official rice area is used to compare with satellite-derived rice areas.

3.3. Proposed method

The proposed method includes four main parts. Firstly, all Landsat 8 SR images are fed to compositing process to create a dense time series of cloud-free Landsat 8 images, i.e up to five images which is distributed across classification year (2016). After that, the composited images are used to extract spectral-temporal features. There will be three independent classifications. The first is classification using single image only (single-image classification), the second classification uses the whole time-series images with a single classifier (XGBoost), last classification is an improved version of the second classification with an addition of more features and ensemble of more strong classifiers. Finally, those classification models are validated against the testing data and statistical data as presented in previous sections.

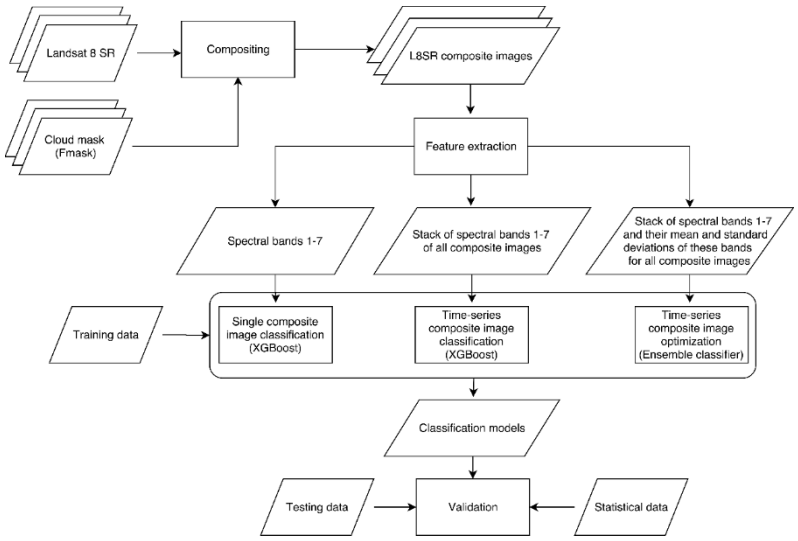

Figure 1. Overall flowchart of the method

3.3.1. Generation of composite images

The purpose of this step is to generate a dense, cloud-free time series to capture major spectral variations for 2016 land cover classification. The target images for compositing were the 5 clearest L8SR images from: 16th May 2016 (DOY 137), 1st June 2016 (DOY 153), 17th June 2016 (DOY 169), 21st September 2016 (DOY 265), and 7th October 2016 (DOY 281). These images were the targets for the compositing process which replaces their own cloud/cloud shadow pixels with best quality pixels from the above potential candidate images based on a scoring method described below.

For each target image, clear pixels remain while cloudy pixels are replaced by a clear observation selected from the candidates. I

combine two BAP methods proposed in Griffiths et al. (2013) and White et al. (2014) and modify the opacity score for compatibility with L8SR data. For each clear pixel in a candidate image, a score is computed based on 4 sub-scores: year score, DOY score, opacity score and distance from cloud/cloud shadow pixel. Year score, DOY score and distance to cloud/cloud shadow are computed following Griffiths et al. (2013). Year scores decrease with distance from target year (2016) to support years (2015, 2014, 2013). DOY scores reflect ranges of target day and support days following Gaussian distribution. Distance to cloud/cloud shadow is calculated by a Sigmoid function of distances from the pixel to cloud/cloud shadow, obtained from the file sr_cfmask (Zhu, Wang, and Woodcock 2015), in radius of 50 pixels around. The opacity score requires an aerosol image as input (White et al. 2014), but L8SR provides only discrete aerosol information (i.e. 4 aerosol levels) in the sr_cloud files. Therefore, I assign opacity scores to the aerosol levels using a Sigmoid function. Finally, a pixel's score is derived by summing the four sub-scores. The candidate pixel owning the greatest score is chosen to replace the clouded pixel in the target image (Table 5).

3.3.2. Land cover classification

Three classification methods are investigated as in Figure 2. First, an XGBoost classifier is applied on 7 spectral bands of each composite image to obtain 5 LC maps for 2016. The second is time-series classification using XGBoost classifier on stack of 7 spectral bands of 5 composites (i.e. 35 spectral-temporal features). After that, they are

compared to assess if a time-series of composites is better than individual composites for classification. The third improves the time-series composite classification by adding Mean Standard Deviations (MSDs) of each band calculated from the composites. Five single classifiers (XGBoost, LR, SVM-RBF, SVM-Linear and MLP) and an ensemble model using majority voting (i.e. predicted class labels are voted by five classifiers having the same weight) are compared. The selection of these classifiers is due to wide applications for LCC using SVM and MLP (Foody and Mathur 2004; Kavzoglu and Mather 2003) and LR (Mallinis and Koutsias 2008) reported in literature. Additionally, XGBoost is investigated due to novelty (Chen and Guestrin 2016) and current lack of LCC applications.

All of these classifiers have specific hyper-parameters that require tuning for the best classification performance. Specifically, SVM-RBF's hyper-parameters are penalty (C) and gamma. SVM-Linear requires penalty (C) only. Important hyper-parameters forming a base architecture of MLP include activation function (activation), number of hidden layers (hidden layers) and number of hidden nodes in individual hidden layers (hidden nodes). Similar to SVM, LR also has a regularization parameter (C) for individual training data importance (Hackeling 2017). XGBoost has many hyper-parameters in which the three most important ones are the number of boosted trees (n_estimators) and two others for over-fitting prevention: maximum tree depth (max_depth) and minimum sum of weights of all observations required in a child (min_child_weight).

All classifications were performed on the same training and testing points with 10-fold cross validation to select best hyper-parameters for each classifier. Then all training data is used to train classifiers with best parameters. Testing sets are separated from training sets to assess trained classifiers. I used scikit-learn implementation of the classifiers in our experiments (http://scikit-learn.org). Scikit-learn is a python-based machine learning library with robust tools and easy-to-use interface.

3.4. Metrics for classification assessment

Overall accuracy (OA), kappa coefficient, producer accuracy (PA), user accuracy (UA) and F1 score (F1) are used as evaluation metrics in this study [34], [35]. OA and kappa coefficient are computed for classification level.

CHAPTER 4. EXPERIMENTS AND RESULTS

4.1. Compositing results

Before composition, the average cloud percentage over 5 target images is 20.54% where image at DOY 169 is cloudiest with 73.63% cloud pixels. After compositing, all images are at least 99.78% clear (i.e. DOY 265). However, there are remaining cloudy pixels without replacement candidates. 2015 data mostly contributes to composition with 72.36%, followed by 2013 (22.04%), 2014 (5.55%) and 2016

(0.05%) data.

Although pixel candidates are carefully selected by BAP, they are still spectrally different from neighbouring pixels of other candidate images. For example, for DOY 265 in Figure 4b, composite pixels over a rice planting area show different colour blocks. Some cloudy pixels are replaced by vegetated observations while others are replaced by flooded observations. This indicates selection of appropriate images has significant impact on BAP composites for areas with a high temporal dynamic of land-cover types, especially rice and agricultural areas. Thus, knowledge of local agricultural calendar could improve image selection for spectrally-uniform BAP composites.

NDVI and Bare Soil Index (BSI) temporal profiles of seven land cover classes are presented in Figure 14. Seven classes can be divided into four distinct groups: (impervious area, bare land), paddy rice, water, and (tree, crop, grass and shrub). Due to cultivation practices, paddy rice's NDVI and BSI temporal profile varies across the year.

4.2. Assessment of land-cover classification based on point validation

4.2.1. Yearly single composite classification versus yearly time-series composite classification

Test set validation results are provided in Table 5. I found classifications using time-series composites outperformed all single-image classifications with 10.03% higher OA and 0.13 higher kappa

coefficient on average. Single-image classification is also unstable as the results range from 68.43 – 76.38% for OA, 0.59 –0.68 for kappa coefficient. I found 3 out 5 single-image classifications achieved greater than 72% OA, except for the DOY169 and DOY265 which have large BAP pixels included with 73.60% and 24.76% respectively.

Table 1. F1 score, F1 score average, OA and kappa coefficient for 7 land cover classes of six classification cases obtained using XGBoost. Best classification cases are written in bold.

	DOY 137	**DOY 153**	**DOY 169**	**DOY 265**	**DOY 281**	**Time series**
Crop	0.50	0.39	0.36	0.33	0.40	**0.58**
Bare land	0.06	**0.26**	0.04	0.17	0.14	0.22
Paddy rice	0.87	0.84	0.81	0.73	0.80	**0.91**
Water	0.85	0.86	0.73	0.81	0.83	**0.91**
Tree	0.67	0.70	0.66	0.65	0.74	**0.80**
Impervious area	0.84	0.87	0.78	0.83	0.86	**0.90**
Grass/Shrub	0.36	0.29	0.30	0.27	0.28	**0.44**
F1 score average	0.76	0.74	0.69	0.68	0.73	**0.82**
OA (%)	76.4	75.7	69.7	68.4	73.6	**82.8**
kappa coefficient	0.68	0.68	0.61	0.59	0.66	**0.77**

Considering per-class accuracy, classification of vegetation classes

are significantly improved with time series classification, as those classes have high temporal dynamics best captured by multiple observations (Arvor et al. 2011; Kontgis, Schneider, and Ozdogan 2015). From the results, rice in green stage in DOYs of 137, 153, 265 is most confused with crop and grass/shrub. In DOY 169, rice fields are flooded, thus resulting in confusion of rice and water. In the last image, DOY 281, harvested rice is confused with bare land and impervious area. By integrating all confusing information in time-series classification, rice are better separated from other vegetation classes with F1=0.91.

Although most LC classes are better identified in time-series classification, bare land had confusion with impervious area (maximum F1=0.26, the time-series F1=0.22). This is attributed to the two classes having spectrally similar and stable reflectance through time, and a low number of training samples for bare land. Crop and grass/shrub are occasionally misclassified due to similar spectral signals and mixed pixels. Water is separable from other classes due to its unique spectral properties, but some water bodies are seasonally vegetated, leading to misclassification of water and vegetation. Thus, water also benefits from multiple image observations.

4.2.2. Improvement of ensemble model against single-classifier model

For ensemble classification, the following single models with their optimized parameters are employed: i) XGBoost with

n_estimators=1000, max_depth=5, min_child_weight=1; ii) LR with C=1; iii) SVM-RBF with C=10, gamma=0.03125; iv) SVM-Linear with C=8; v) MLP with activation=tank, hidden layers=1, and hidden nodes=40. Classifiers perform on a stack of 35 spectral temporal features and 7 MSDs of spectral bands. Majority voting technique is employed for the ensemble model.

Table 2. OA, kappa coefficient, F1 score average for each single-classifier and ensemble model. Best classification cases are written in bold.

Measure	**Classifier**					
	XGBoost	**LR**	**SVM-RBF**	**SVM-Linear**	**MLP**	**Ensemble**
OA (%)	83.2	82.6	82.9	81.9	83.1	**84.0**
kappa coefficient	0.77	0.77	0.78	0.77	0.78	**0.79**
F1 score average	0.82	0.82	0.83	0.83	0.83	**0.84**

Using an ensemble of supervised classifiers improves the classification (Table 3). I found individual models have similar accuracies with SVM-Linear is the lowest at 81.94% OA and XGBoost is the highest with 83.23% OA. The ensemble model is better than all individual models with OA=83.96% and kappa coefficient=0.79. Per-class accuracies of the ensemble model filter the best results from all single-classifier models. Classifier F1 score performance is presented in Figure 16.

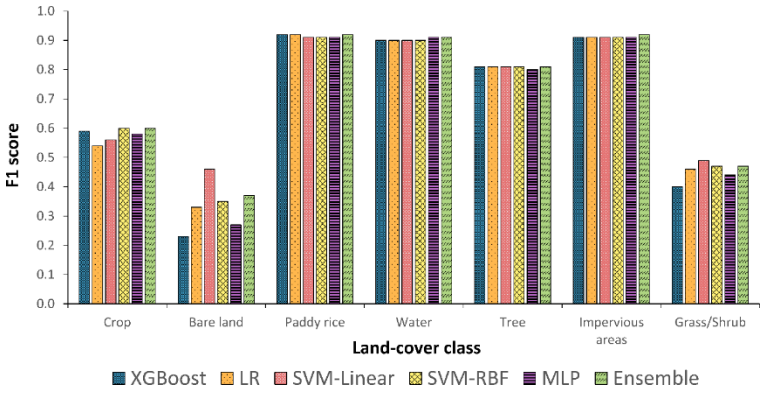

Figure 2. F1 score for land-cover class obtained using multiple classifiers.

XGBoost is not effective at classifying bare land (F1=0.23) and grass/shrub (F1=0.4), but this disadvantage is overcome by SVM-RBF and SVM-Linear with F1 of 0.35, 0.46 for bare land and 0.47, 0.49 for grass/shrub respectively. SVM-RBF and SVM-Linear are generally high performing. Paddy rice, impervious area, water and tree have similar accuracies between classifiers which could be explained as the classes are quite separable in this time-series domain. MLP is overall good compared to other classifiers, but it performs poorly on bare land (F1 = 0.27). Ensemble model achieved similar accuracies of paddy rice, water, tree and impervious areas as compared to other classifiers. However, for crop, grass/shrub and bare land which are easily confused with other classes (Figure 15), ensemble model generally achieved better classification accuracies than any single-classifier model. By integrating models, individual strengths remain, while weaknesses are reduced. Table 4 presents confusion matrix of the ensemble model with User Accuracy (UA) and Producer Accuracy (PA) for each class.

Table 3. Confusion matrix of ensemble model.

	Crop	Bare land	Rice	Water	Tree	Impervious	Grass/Shrub	Reference total	UA (%)
Crop	**222**	3	25	4	24	22	31	331	66.1
Bare land	6	**22**	1	1	0	22	4	56	33.5
Rice	37	0	**581**	16	2	3	7	646	91.6
Water	5	0	11	**411**	4	11	4	446	90.9
Tree	26	2	3	2	**433**	8	17	491	83.2
Impervious	19	6	4	3	5	**485**	1	523	93.1
Grass/Shrub	56	7	12	5	47	11	**117**	255	38.9
Classification total	371	40	637	442	515	562	181	**2748**	**OA (%)**
PA (%)	55.1	41.0	92.8	92.0	79.3	90.5	59.8	**OA (%)**	**84.0**

4.3. Assessment of land-cover classification results based on map validation

The LC map of the ensemble model is displayed in Figure 17. I found that paddy rice and impervious area are the dominant classes.

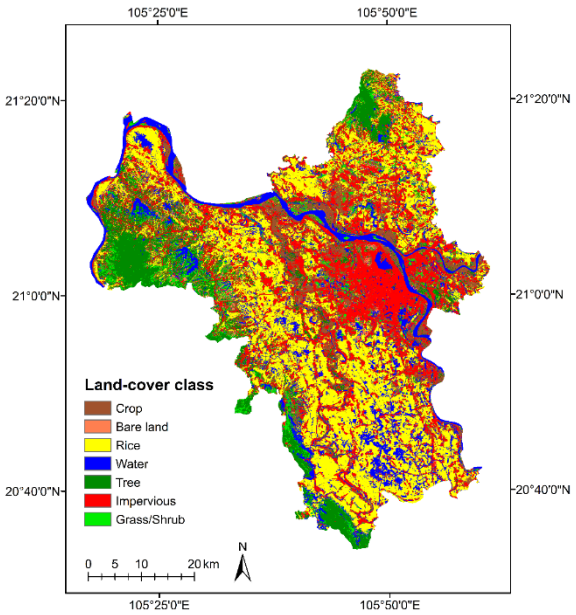

Figure 3. 2016 Land-cover map for Hanoi based on the most accurate classification using time-series composite imagery and the ensemble of five classifiers.

According to (Office 2016), rice area in Hanoi for the spring-summer season is approximately 99,454 ha. I computed rice area for the classification maps and compared to the official statistic. The ensemble rice map is closest to the official number, and slightly overestimates by 4,764 ha (4.79%). Additional classifiers are shown in (Table 9).

To summary, the best land-cover map using the ensemble model achieved 83.91% OA with kappa coefficient of 0.79. This is in comparison to 72% OA using the unmodified compositing algorithm in a slightly larger region and a few additional land cover types [20]. Additional regional land cover mapping studies had generally good

accuracy with: 89% OA for forest/non-forest cover maps [19], 90% OA for urban landscape with dense time-series stack [36], 89% OA for land cover map in a less-cloudy region with automated pre-processing and random forest [37], 89.42% OA in a recent rice/non-rice cover study over Red River Delta with dense Landsat 8 time-series stack [38], and 84% OA in a recent land cover study over Hanoi employing radar to overcome clouds [39].

Multi-year composition increases cloud-free pixels in composites, especially over cloud-persistent areas such as Hanoi, Vietnam. A time-series composites with over 99% cloud-free pixels was developed. One disadvantage of this compositing is that it does not account for intra-annual vegetation phenology. However, using time-series composites still improves classification performance in comparison with any single composite classification. This is attributed to the effective representation of seasonal temporal dynamics of land-cover types. Among the top supervised classifiers, XGBoost performed best for land cover mapping. However, an ensemble model still improved classification results by promoting individual strengths and reducing weaknesses. This ensemble model is especially effective for confusing classes (bare land, crop, grass/shrub) but not already well-separated classes (paddy rice, water). In the future, image composition accounting for phenology could improve composite quality and classification accuracy for improved mapping of land cover types with high temporal dynamics.

CHAPTER 5. CONCLUSION

In this thesis, I have conducted a research on land cover classification using Landsat 8 satellite images. Specifically, I have presented in this thesis: (i) fundamental concepts of remote sensing sciences, (ii) satellite images and its applications in various domains,

(iii) land cover classification problems. A comprehensive review of land cover classification methods has been conducted to address its current developments. LCC is a traditional application in remote sensing. Many LCC studies have been conducted in different places on Earth. However, LCC using optical satellite images in cloud-prone areas with high temporal dynamics of land covers is still challenging due to lack of cloud-free data. In this thesis, I have proposed a LCC method for these areas. The result of this research is also published in the *International Journal of Remote Sensing (Taylor & Francis)* in a paper entitled "*Improvement of land-cover classification over frequently cloud-covered areas using Landsat 8 time-series composites and an ensemble of supervised classifiers*".

In this thesis, I have proposed a LCC method for these areas. Firstly, a dense time-series of composite images was constructed from all available multi-year Landsat 8 images over the study area. A modified compositing method was proposed for the compositing process using Landsat 8 SR images. The result images are almost cloud-free thus are ready for feature extraction. An ensemble of five experimentally strongest supervised classifiers in the experiments was built to classify a stack of composite images and additional features (Mean Standard Deviations). The best land-cover map achieved 83.91% OA with kappa coefficient of 0.79. Some conclusions could be drawn from the research including: (i) multi-year composition increases cloud-free pixels in composites, especially over cloud-persistent areas such as Hanoi, Vietnam; (ii) accurate land cover maps could be derived from time-series composite images; (iii) ensemble

learning could slightly improve classification as compared to any single-classifier model, however, significant improvements are observed for confusing classes as in single model, but not for well-separated classes.

There are also some remaining problems including: (i) The compositing method does not account for intra-annual vegetation phenology thus may not be good enough for some land covers like paddy rice; (ii) there are still significant confusions between bare land/impervious surface, grass/crops/trees due to their similar spectral characteristics, even in temporal domain. Therefore, future researches could be placed on improvement of compositing methods for high temporal dynamics land covers. And development of LCC methods for better separating of bare land/impervious surface, grass/crops/trees.

Reference

[1] *Fundamentals of Remote Sensing*. .

[2] K. Hibbard *et al.*, "Research priorities in land use and land-cover change for the Earth system and integrated assessment modelling," *Int. J. Climatol.*, vol. 30, no. 13, pp. 2118–2128,

Nov. 2010.

[3] T. Kuemmerle *et al.*, “Challenges and opportunities in mapping land use intensity globally,” *Curr. Opin. Environ. Sustain.*, vol. 5, no. 5, pp. 484–493, 2013.

[4] H. Müller, P. Rufin, P. Griffiths, A. J. Barros Siqueira, and P. Hostert, “Mining dense Landsat time series for separating cropland and pasture in a heterogeneous Brazilian savanna landscape,” *Remote Sens. Environ.*, vol. 156, pp. 490–499, 2015.

[5] X. Zhang, D. Pan, J. Chen, Y. Zhan, and Z. Mao, “Using long time series of Landsat data to monitor impervious surface dynamics: a case study in the Zhoushan Islands,” *J. Appl. Remote Sens.*, vol. 7, no. 1, p. 73515, 2013.

[6] D. Arvor, M. Jonathan, M. S. P. Meirelles, V. Dubreuil, and L. Durieux, “Classification of MODIS EVI time series for crop mapping in the state of Mato Grosso, Brazil,” *Int. J. Remote Sens.*, vol. 32, no. 22, pp. 7847–7871, 2011.

[7] M. A. Wulder, J. G. Masek, W. B. Cohen, T. R. Loveland, and C. E. Woodcock, “Remote Sensing of Environment Opening the archive : How free data has enabled the science and monitoring promise of Landsat,” *Remote Sens. Environ.*, pp. 1–9, 2012.

[8] T. Le Toan *et al.*, “Rice crop mapping and monitoring using ERS-1 data based on experiment and modeling results,” *IEEE Trans. Geosci. Remote Sens.*, vol. 35, no. 1, pp. 41–56, 1997.

[9] C. Kontgis, A. Schneider, and M. Ozdogan, “Mapping rice paddy extent and intensification in the Vietnamese Mekong River Delta with dense time stacks of Landsat data,” *Remote Sens. Environ.*, vol. 169, pp. 255–269, 2015.

[10] A. K. Whitcraft, E. F. Vermote, I. Becker-Reshef, and C. O. Justice, “Cloud cover throughout the agricultural growing season: Impacts on passive optical earth observations,” *Remote Sens. Environ.*, vol. 156, pp. 438–447, 2015.

[11] T. T. N. Nguyen *et al.*, “Particulate matter concentration mapping from MODIS satellite data: a Vietnamese case study,” *Environ. Res. Lett.*, vol. 10, no. 9, p. 95016, Sep. 2015.

[12] N. D. Duong, “Study of Land Cover Change in Vietnam for the Period 2001-2003 Using Modis 32 Days Composite,” no. May, 2003.

[13] L. T. Ngo, D. S. Mai, and W. Pedrycz, “Semi-supervising Interval Type-2 Fuzzy C-Means clustering with spatial information for multi-spectral satellite image classification and change detection,” *Comput. Geosci.*, vol. 83, pp. 1–16, 2015.

[14] L. Henits, C. Jürgens, and L. Mucsi, “Seasonal multitemporal land-cover classification and change detection analysis of Bochum, Germany, using multitemporal Landsat TM data,” *Int. J. Remote Sens.*, pp. 1–16, Jan. 2016.

[15] J. C. White *et al.*, “Pixel-based image compositing for large-area dense time series applications and science,” *Can. J. Remote Sens.*, vol. 40, no. 3, pp. 192–212, 2014.

[16] J. Cihlar, D. Manak, and M. D’Iorio, “Evaluation of compositing algorithms for AVHRR data over land,” *IEEE Trans. Geosci. Remote Sens.*, vol. 32, no. 2, pp. 427–437, Mar. 1994.

[17] “An overview of MODIS Land data processing and product status,” *Remote Sens. Environ.*, vol. 83, no. 1–2, pp. 3–15, Nov. 2002.

[18] D. P. Roy *et al.*, “Web-enabled Landsat Data (WELD): Landsat ETM+ composited mosaics of the conterminous United States,” *Remote Sens. Environ.*, vol. 114, no. 1, pp. 35–49, 2010.

[19] P. Potapov, S. Turubanova, and M. C. Hansen, “Remote Sensing of Environment Regional-scale boreal forest cover and change mapping using Landsat data composites for European Russia,” *Remote Sens. Environ.*, vol. 115, no. 2, pp. 548–561, 2011.

[20] P. Griffiths, S. Van Der Linden, T. Kuemmerle, and P. Hostert, "A pixel-based landsat compositing algorithm for large area land cover mapping," *IEEE J. Sel. Top. Appl. Earth Obs. Remote Sens.*, vol. 6, no. 5, pp. 2088–2101, 2013.

[21] C. Gómez, J. C. White, and M. A. Wulder, "Optical remotely sensed time series data for land cover classification : A review," *ISPRS J. Photogramm. Remote Sens.*, vol. 116, pp. 55–72, 2016.

[22] H. S. J. Zald *et al.*, "Integrating Landsat pixel composites and change metrics with lidar plots to predictively map forest structure and aboveground biomass in Saskatchewan, Canada," *Remote Sens. Environ.*, vol. 176, pp. 188–201, Apr. 2016.

[23] S. D. Thompson, T. A. Nelson, J. C. White, and M. A. Wulder, "Mapping Dominant Tree Species over Large Forested Areas Using Landsat Best-Available-Pixel Image Composites," *Can. J. Remote Sens.*, vol. 41, no. 3, pp. 203–218, May 2015.

[24] P. D. Pickell, T. Hermosilla, R. J. Frazier, N. C. Coops, and M. A. Wulder, "Forest recovery trends derived from Landsat time series for North American boreal forests," *Int. J. Remote Sens.*, vol. 37, no. 1, pp. 138–149, Jan. 2015.

[25] T. Hermosilla, M. A. Wulder, J. C. White, N. C. Coops, and G. W. Hobart, "An integrated Landsat time series protocol for

change detection and generation of annual gap-free surface reflectance composites," *Remote Sens. Environ.*, vol. 158, pp. 220–234, Mar. 2015.

[26] S. E. Franklin, O. S. Ahmed, M. A. Wulder, J. C. White, T. Hermosilla, and N. C. Coops, "Large Area Mapping of Annual Land Cover Dynamics Using Multitemporal Change Detection and Classification of Landsat Time Series Data," *Can. J. Remote Sens.*, vol. 41, no. 4, pp. 293–314, Jul. 2015.

[27] G. Li, D. Lu, E. Moran, and S. J. S. Sant'Anna, "Comparative analysis of classification algorithms and multiple sensor data for land use/land cover classification in the Brazilian Amazon," *J. Appl. Remote Sens.*, vol. 6, no. 1, p. 61706, Dec. 2012.

[28] G. M. Foody and A. Mathur, "A relative evaluation of multiclass image classification by support vector machines," *IEEE Trans. Geosci. Remote Sens.*, vol. 42, no. 6, pp. 1335–1343, 2004.

[29] G. Mallinis and N. Koutsias, "Spectral and Spatial-Based Classification for Broad-Scale Land Cover Mapping Based on Logistic Regression," *Sensors*, pp. 8067–8085, 2008.

[30] T. Kavzoglu and P. M. Mather, "The use of backpropagating artificial neural networks in land cover classification," *Int. J. Remote Sens.*, no. December 2014, pp. 37–41, 2003.

[31] M. Pal and P. M. Mather, “Support vector machines for classification in remote sensing,” *Int. J. Remote Sens.*, no. March 2013, pp. 37–41, 2006.

[32] Government of Vietnam, “Resolution on landuse planning from 2011-2015 and by 2020 for Hanoi.” 2013.

[33] Hanoi Environment and Natural Resources Department, “Land use statistics of Hanoi,” 2010. [Online]. Available: http://qhkhsdd.hanoi.gov.vn.

[34] R. G. Congalton and K. Green, *Assessing the Accuracy of Remotely Sensed Data: Principles and Practices*. CRC Press, Taylor & Francis Group, Boca Raton, 2008.

[35] D. M. W. Powers, “Evaluation: From Precision, Recall and F-Measure To Roc, Informedness, Markedness & Correlation,” *J. Mach. Learn. Technol.*, vol. 2, no. 1, pp. 37–63, 2011.

[36] M. Castrence, D. Nong, C. Tran, L. Young, and J. Fox, “Mapping Urban Transitions Using Multi-Temporal Landsat and DMSP-OLS Night-Time Lights Imagery of the Red River Delta in Vietnam,” *Land*, vol. 3, no. 1, pp. 148–166, 2014.

[37] B. Mack, P. Leinenkugel, C. Kuenzer, and S. Dech, “A semi-automated approach for the generation of a new land use and land cover product for Germany based on Landsat time-series

and Lucas *in-situ* data," *Remote Sens. Lett.*, vol. 8, no. 3, pp. 244–253, Mar. 2017.

[38] N. T. N. T. Man Duc Chuc, Nguyen Hoang Anh, Nguyen Thanh Thuy, Bui Quang Hung, "Paddy Rice Mapping in Red River Delta region Using Landsat 8 Images : Preliminary results," *9th Int. Conf. Knowl. Syst. Eng. (KSE 2017)*, 2017.

[39] D. Nguyen, W. Wagner, V. Naeimi, and S. Cao, "Rice-planted area extraction by time series analysis of ENVISAT ASAR WS data using a phenology-based classification approach: A case study for Red River Delta, Vietnam," in *Proceedings of the International Archives Photogrammetry, Remote Sensing and Spatial Information Science, Berlin, Germany*, 2015.